Received: 2 July 2020 | Revised: 22 March 2021 | Accepted: 6 April 2021

DOI: 10.1049/smt2.12066

IET Science, Measurement & Technology

The Institution of Engineering and Technology WILEY

ORIGINAL RESEARCH PAPER

Analysis of hybrid polarization frequency domain spectrum characteristics of oil-paper insulation transformers

Yang Zou[1] | Jin He[1] | Qianlin He[1] | Mengqi Wang[2]

[1] College of Electrical Engineering and Automation, Fuzhou University, Fuzhou, China

[2] Department of Electrical and Computer Engineering, University of Michigan-Dearborn, Dearborn, USA

Correspondence
Mengqi Wang, Department of Electrical and Computer Engineering, University of Michigan-Dearborn, Dearborn, USA.
Email: mengqiw@umich.edu

Funding information
Natural Science Foundation of Fujian, Grant/Award Number: 2019J01248; Science Development Foundation of Fuzhou University, Grant/Award Number: GXRC-18070; Natural Science Foundation of Fujian, Grant/Award Number: 2019J01248; Science Development Foundation of Fuzhou University, Grant/Award Number: GXRC-18070

Abstract

This paper utilizes a hybrid Debye model to accurately simulate the relaxation response process of the oil-paper insulation of a transformer to explore the application of frequency domain dielectric spectroscopy (FDS) in nondestructive diagnosis of the aging condition of oil-paper insulation. Via FDS test data, the model parameters can be identified, and the influence laws of FDS can be obtained through the variation of model parameters. To explore the effects of insulating paper moisture content, insulating paper layers, and test temperature on FDS characteristics, an FDS experimental platform is established. The results show that the hybrid Debye model can effectively reflect the relaxation response process of oil-paper insulation under different conditions, as well as that a physical relationship between the model parameters and oil-paper dielectric polarization exists. In addition, the parameters of the hybrid Debye model can be used as the characteristic quantities for the non-destructive evaluation of the oil-paper insulation state, providing new ideas for the non-destructive evaluation of the oil-paper insulation state.

1 | INTRODUCTION

As the pivotal equipment of a power system, the power transformer is the key to ensuring the stability, reliability, and safety of a power system. Since aging and dampening of the oil-paper insulation system are the main cause of transformer failure [1–6], it is particularly important to reasonably, effectively, nondestructively, and comprehensively diagnosis the state of the oil-paper insulation system. Doing so has great practical significance and economic benefits.

The measurement conclusions of RVM [7–11] (return voltage method), PDC [12–16] (polarization and depolarization current), and FDS [17–23] (frequency domain spectroscopy) based on dielectric response are consistent when it comes to transformer aging diagnosis. RVM can only evaluate the overall condition of the insulation and cannot distinguish the condition of insulating oil from that of insulating paper. Moreover, it is susceptible to the accuracy limitation of signal measurement and electromagnetic interference in the time domain, making interpretations of experimental results very complicated [7, 8]. PDC, on the other hand, has certain advantages in diagnosing the insulation state of transformers. However, when measuring the polarization and depolarization current for a long time, the long test process and the large temperature variation will seriously affect the measurement results. Moreover, the field test will inevitably be affected by electromagnetic interference because the polarization and depolarization current values are quite small, the accuracy of the measurement is questionable in this case. Therefore, how to suppress the field temperature interference and electromagnetic interference needs to be further studied [14, 15]. Meanwhile, FDS, as a nondestructive electrical diagnosis technology, has the characteristics of a strong anti-interference ability, wide measurement frequency band, and abundant information compared to the other methods [18–29].

The research method based on FDS test data can be summarized as follows. First, the characteristics are extracted directly from the FDS curve to find the relationship between the characteristics and the insulation characteristics. The second is to establish an equivalent model of the oil-paper insulation system

This is an open access article under the terms of the Creative Commons Attribution License, which permits use, distribution and reproduction in any medium, provided the original work is properly cited.
© 2021 The Authors. *IET Science, Measurement & Technology* published by John Wiley & Sons Ltd on behalf of The Institution of Engineering and Technology

based on the FDS measurement curve, and to explore the change rule of the oil-paper insulation characteristics reflected by the model parameter changes. The latter has received extensive attention and research due to its specific microphysical theoretical basis to explain the change of dielectric insulation characteristics. At present, the equivalent models used in oil paper insulation system mainly include extended Debye model (EDM), Maxwell Wagner model, X–Y model, Cole–Cole model and so on. Bognar et al. [25] utilized the extended Debye model consisting of a few RC branches to monitor the insulation state of equipment. However, in the actual polarization process of transformer oil paper insulation system, insulation oil, insulation paper and a series of aging products will form interface polarization [27]. Obviously the application of EDM ignores the existence of interface polarization. The Maxwell–Wagner model [26], composed of two RC series circuits, can be used to calculate voltage distribution and dielectric loss, but its calculation accuracy is limited, owing to its neglect of the nonlinear characteristics of resistance and the relaxation process [27–29]. Besides, Zhang et al. [30] used the X–Y model to simulate the polarization characteristics of the complex oil-paper insulation structure, which is composed of separators, oil gaps, and braces. X–Y model can better reflect the structure of oil paper insulation system. However, in some early transformers, it is difficult to know the size parameters of oil paper insulation, so the parameters of X–Y model can not be accurately obtained. Ojha et al. [31] drew the Cole–Cole circle of the repolarization rate of oil-paper insulation, and found that the insulation state is obviously related to the size, relaxation time, and distribution parameters of the Cole-Cole circle. However, the distribution parameters of Cole–Cole model has no physical meaning and can not further explain the polarization process of oil paper insulation. During the operation of oil paper insulation, a series of aging products (including water, acid etc.) are produced. The relative dielectric constant of these products are different, so complex interface polarization are formed. Moreover, the uneven distribution of water in the material also makes the polarization process of the dielectric more complex [32–33]. The interface polarization process of oil-paper insulation is very important for judging the degree of moisture and aging of oil-paper insulation. Therefore, it is necessary to establish an equivalent model that can accurately reflect the interface polarization process of oil-paper insulation.

Based on the above background, this paper presents a hybrid Debye model (HDM) to reflect the complex polarization process of oil-paper insulation, which appends hybrid branches to characterize complex interface reactions on account of the difference between the interface polarization and dielectric polarization. This paper is organized as follows. First, the construction of the hybrid Debye model based on FDS and the identification of its parameters are introduced; then the relationship between the equivalent model parameters and the polarization process of the oil-paper insulation system is explored through the simulation platform; finally, the effects of different external factors on the oil-paper insulation system are analysed through experiments. The influence of the FDS spectral line of the insulating sample, and the establishment of the HDM model, and verify the accuracy and validity of the equivalent model through the degree of agreement.

2 | HYBRID DEBYE MODEL AND PARAMETER IDENTIFICATION BASED ON FDS

The equivalent circuit model of HDM is shown in Figure 1. In Figure 1, the HDM of the oil-paper insulation includes a geometric equivalent circuit, k interface RC series polarization branches, and n interface polarization branches. R_g, C_g, $R_{pi}(i = 1, 2, \ldots, k)$, $C_{pi}(i = 1, 2, \ldots, k)$, $R_{b(2j-1)}(j = 1, 2, \ldots, n)$, $R_{b(2j)}(j = 1, 2, \ldots, n)$, and $C_{bj}(j = 1, 2, \ldots, n)$ are insulation resistance, geometric capacitance, polarization resistances, polarization capacitances, interfacial polarization resistances, and interfacial polarization capacitances, respectively.

The various code symbols mentioned in this paper and their corresponding meanings are shown in Table 1.

According to dielectric physics theories [34], the relationship between the equivalent admittance Y of the HDM and complex capacitance C are expressed as:

$$Y = j\omega C = j\omega(C'(\omega) - jC''(\omega)) \tag{1}$$

In terms of the Maxwell circuit principle [35], the real part of dielectric complex capacitance C' can be described as:

$$C'(\omega) = C_g + \sum_{i=1}^{k} \frac{C_{pi}}{1 + (\omega\tau_i)^2} + \sum_{j=1}^{n} \frac{\tau_i^2}{(1 + \omega^2\tau_j{}^2)R_{b(2j-1)}^2 C_{b(2j)}} \tag{2}$$

The imaginary part of dielectric complex capacitance C′′ is depicted as:

$$C''(\omega) = \frac{1}{\omega R_g} + \sum_{i=1}^{k} \frac{\omega\tau_i C_{pi}}{1 + (\omega\tau_i)^2} + \sum_{j=1}^{n} \frac{\omega^2\tau_j^2(R_{b(2j-1)} + R_{b(2j)}) + R_{b(2j-1)}}{(\omega + \omega^3\tau_j^2)R_{b(2j-1)}(R_{b(2j-1)} + R_{b(2j)})} \tag{3}$$

In Equations (2)–(3), the time constant τ is denoted as:

$$\begin{cases} \tau_i = R_{pi}C_{pi} & i = 1, 2, \ldots, k \\ \tau_j = \dfrac{R_{b(2j-1)}R_{b(2j)}}{R_{b(2j-1)} + R_{b(2j)}} C_{bj} & j = 1, 2, \ldots, n \end{cases} \tag{4}$$

The dielectric loss factor, tan δ, can be derived from the ratio of the imaginary part to the real part of the complex capacitance,

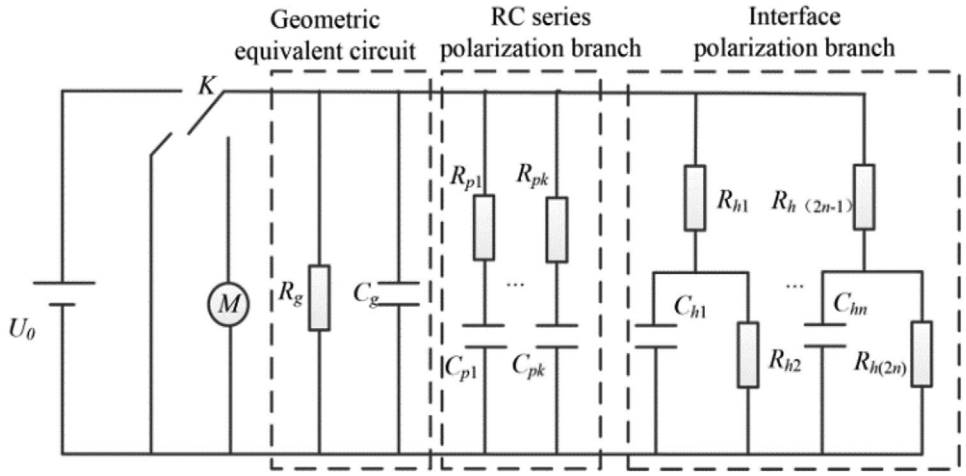

FIGURE 1 Hybrid Debye model equivalent circuit

TABLE 1 Code symbols and corresponding meanings

Code symbol	Corresponding meaning
R_g	insulation resistance
C_g	geometric capacitance
R_{pi}	polarization resistances
C_{pi}	polarization capacitances
$R_{h(2j-1)}$ or $R_{h(2j)}$	interfacial polarization resistances
C_{hi}	interfacial polarization capacitances
ω	frequency
Y	equivalent admittance
C'	real part of dielectric complex capacitance
C''	imaginary part of dielectric complex capacitance
τ	time constant
tan δ	dielectric loss factor
W	consistency

and is represented as:

$$\tan\delta = \frac{C''(\omega)}{C'(\omega)} \tag{5}$$

Furthermore, test and calculated complex capacitance and dielectric loss factor data are selected for parameter identification.

We can also construct the objective optimization function, as shown in Equation (6):

$$y = \min \sum_{i=1}^{m} \left[\left(\tan\delta_M(\omega_i) - \tan\delta_C(\omega_i)\right)^2 + \left(C'_M(\omega_i) - C'_C(\omega_i)\right)^2 + \left(C''_M(\omega_i) - C''_C(\omega_i)\right)^2 \right] \tag{6}$$

where $C^{'}_{M}(\omega_i)$, $C^{''}_{M}(\omega_i)$, $\tan\delta_M(\omega_i)$ are the FDS measured values at each corresponding frequency, and $C^{'}_{C}(\omega_i)$, $C^{''}_{C}(\omega_i)$, and $\tan\delta_C(\omega_i)$ are the calculated values of model equivalent parameters as substituting them into Equations (2)–(5) at each corresponding frequency. The optimal solutions can be obtained as the objective optimization function approaches 0.

TABLE 2 Parameter identification results of the tsja-20/0.5 induction transformer based on the HDM

Equivalent branches		R_i /GΩ	C_i /nF
RC series polarization branches	1	1.575769	0.1668006
	2	2.064331	4.208034
	3	12.48907	46.95477
	4	901.4154	145.4899
Interface polarization branches	1	9.62025651153.9287	0.0001
	2	2.58948984.7425845	37.2908
Geometric branches	/	R_g = 170.6284	C_g = 0.01744

The consistency, W, of comparing the measured and calculated values of each group of characteristic quantities can be extracted as:

$$W = \left(1 - \frac{\sum_{i=1}^{m} |X_C - X_M|}{\sum_{i=1}^{m} X_M}\right) \times 100\% \tag{7}$$

where X_C and X_M are the calculated and measured values of each characteristic quantity. The results with the highest consistency can be selected as the model parameters.

Based on the above strategy, the model parameters of the HDM were identified by FDS test data of a retired oil-immersed induction transformer (TSJA-20/0.5), as shown in Table 2. Model parameters based on the EDM are exhibited in Table 3.

To further demonstrate that the hybrid Debye circuit of oil-paper insulation can more veritably reflect FDS characteristics, a comparison of the consistency between FDS measured values and calculated values obtained from the HDM and the EDM is displayed in Figure 2. In addition, the consistency of different

TABLE 3 Parameter identification results of the tsja-20/0.5 induction transformer based on the EDM

Equivalent branches		R_{pi}/GΩ	C_{pi}/nF
RC series polarization branches	1	0.75373932	0.006894865
	2	1.713349	0.1788665
	3	2.4779937	3.90341
	4	4.8161553	15.05929
	5	4.4776487	304.8654
	6	2006.9082	311.5414
Geometric branches	/	$R_g = 30.5344$	$C_g = 0.013637$

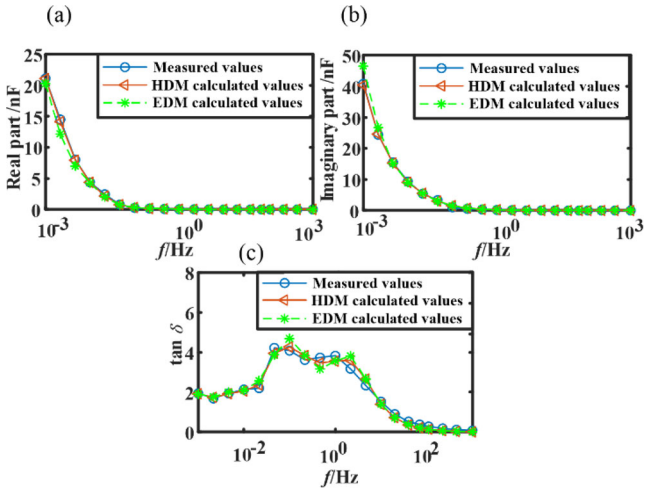

FIGURE 2 Comparison of the consistency between FDS measured values and calculated values: (a) Real part of the complex capacitance; (b) imaginary part of the complex capacitance; (c) tan δ

equivalent models is shown in Table 4, where the consistency of the HDM observably exceeds the consistency of the EDM, thus proving that the HDM possesses greater practicability and superiority compared when with the EDM.

3 | SIMULATION OF FDS CHARACTERISTICS OF OIL-PAPER INSULATION

This simulation study on the influence of the circuit parameters of the HDM on FDS curves lays a foundation for exploring the influence of different environmental factors on FDS characteristics and equivalent model parameters. In the dielectric polarization response process, the insulation system is affected

TABLE 4 The consistency of different equivalent models

Model	Consistency W_1 of C' (%)	Consistency W_2 of C'' (%)	Consistency W_3 of tan δ (%)
HDM	98.06%	97.55%	95.40%
EDM	90.04%	90.32%	88.15%

TABLE 5 Variations of parameters in simulations

	Variations of parameters
Condition 1	$R_g \times 10$
Condition 2	R_g /10
Condition 3	$C_g \times 10$
Condition 4	C_g /10
Condition 5	$R_p \times 10$, C_p/10
Condition 6	R_p /10, $C_p \times 10$
Condition 7	$R_h \times 10$, C_h/10
Condition 8	R_h /10, $C_h \times 10$

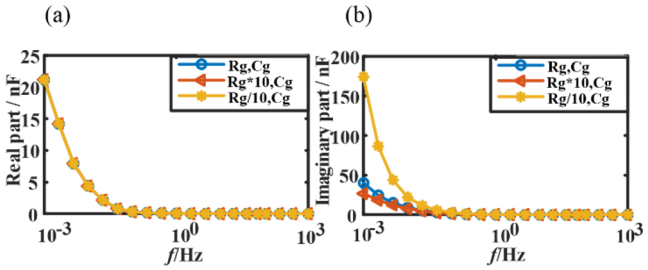

FIGURE 3 Effects of R_g on the complex capacitance curve: (a) Real part; (b) imaginary part

by moisture, aging, and environmental temperature [23]. Hence, FDS characteristics are also affected, which results in the variation of model parameters. To accurately explore the physical relationship among the measured polarization parameters and the dielectric polarization of an oil-paper insulation system, and to determine the effects of the variation of insulation resistance R_g, geometric capacitance C_g, and parameters of the polarization branches on FDS characteristics, simulations were carried out utilizing parameter identification results of a TSJA-20/0.5 induction transformer. R_g, R_p, and Rh decrease while C_g, C_p, and C_h increase with the aging of an oil-paper insulation system [36]. Table 5 shows the variations of the parameters used in simulations.

The real part of the complex capacitance remains constant, and the imaginary part grows with the decrease of R_g in the range of 10^{-3}–10^{0} Hz, as displayed in Figure 3. R_g diminishes with the extension of electric conductivity altered by water, acid, or other aging products produced during the oil-paper insulation aging process, which magnifies the imaginary part of the complex capacitance, while the real part remains immune to the variation.

Figure 4 demonstrates that the real part of the complex capacitance heightens if C_g increases, while the imaginary part is maintained. The enlargement of C_g, owing to storage capacity, was intensified in the period of the insulation state of the transformer turning worse, which lifts the real part of the curve of the complex capacitance, but the imaginary part keeps impregnable.

With the ascent of R_p and the descent of C_p, the real and imaginary parts of the complex capacitance simultaneously rise,

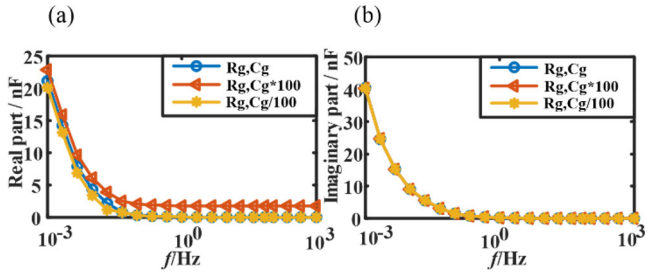

FIGURE 4 Effects of C_g on the complex capacitance curve: (a) real part; (b) imaginary part

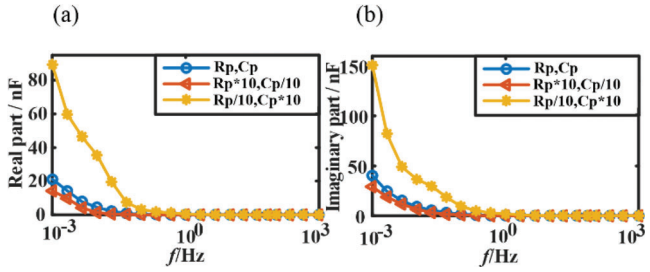

FIGURE 5 Effects of R_b and C_p on the complex capacitance curve: (a) Real part; (b) imaginary part

which is exhibited in Figure 5.Similarly, Figure 6 reveals that the real and imaginary parts of the complex capacitance grow in the process of R_b decreasing and C_b increasing. Furthermore, dielectric polarization and interfacial polarization deepen due to insulation aging, which consequently results in the enhancement of electric conductivity; hence, *as* R_p and R_b decline, C_p and C_b are amplified, which is represented through the rise of the complex capacitance.

4 | EXPERIMENT ON FDS CHARACTERISTICS OF OIL-PAPER INSULATION

In order to verify the effectiveness of HDM, we prepared oil paper insulation samples under different conditions. Figure 7 displays a three-electrode test system, where H, L, and G represent the voltage applying end, the current measuring end,

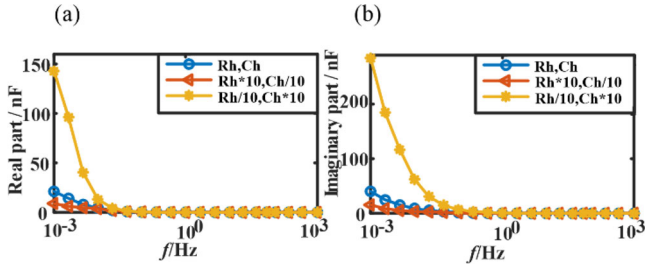

FIGURE 6 Effects of R_b and C_b on the complex capacitance curve: (a) Real part; (b) imaginary part

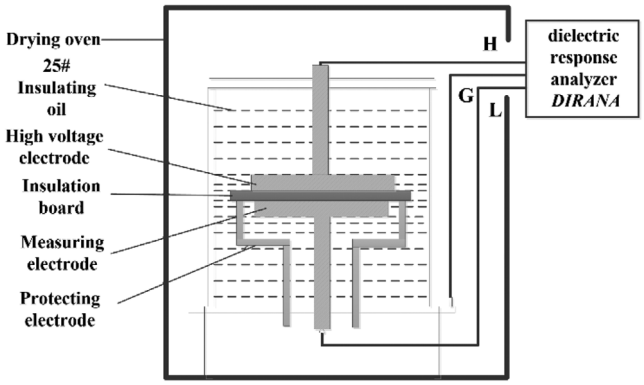

FIGURE 7 Schematic diagram of the FDS test device

and the grounding end, respectively. *OMICRON*'s dielectric response analyser, *DIRANA*, was adopted in the FDS measurement experiment; meanwhile, test frequency, and output voltage peak were individually set at 10^{-3}–10^{3} Hz [3, 22, 33], and 100 V, the frequency sampling points are the default points set by the instrument.

In this experiment, professional insulating boards with a thickness of 1 mm and 25 naphthenic mineral insulating oil were adopted as research objects. First, as part of our preprocessing, the oil-paper insulation samples were pretreated, and the insulating boards were dried for 24 h in a temperature controlled drying oven at 100°C under standard atmospheric pressure. Secondly, the dried insulating boards were placed on the high-precision balance electronic scale to absorb moisture in the air naturally at different times to prepare insulating boards with different moisture gradients. The prepared insulating paper was infused in a hermetic vessel, where degassed mineral oil was injected at 30°C for 48 hours in an oil-paper ratio of 5:1. FDS test data of the samples were employed to explore the influence of moisture content, insulation paper layers, and test temperature on the dielectric properties of oil-paper insulation.

5 | EXPERIMENTAL RESULTS AND ANALYSIS

5.1 | Analysis of FDS data and HDM model parameters of oil paper insulation samples with different moisture content

The oil-paper insulation system of the transformer will be invaded by external moisture and mixed with water molecules produced by the insulation aging of the transformer itself after a long period of service. The moisture content of the paper insulation of transformers will rise from less than 0.5% to more than 4%. Therefore, the moisture content of oil-paper insulation was controlled in 0.1–4% in this experiment. After repeated attempts, the moisture content of the four samples was 0.244%, 1.58%, 2.77%, and 3.63%, respectively, which was measured by a high precision balance electronic scale. The insulation paper

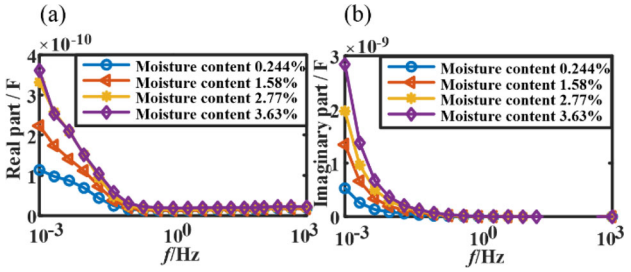

FIGURE 8 Complex capacitance curve under different moisture content: (a) Real part; (b) imaginary part

of the test samples was set to have five layers, and the testing ambient temperature was 30 °C. Moisture produced by the overall aging of an oil-paper insulation system or found in the air is the main factor that damages insulation during the operation of a transformer [15]. An increase in the moisture content of insulation paper leads to an ascent in the number of impurity particles contained in the insulation paper, which in turn leads to the strengthening of the electrical conductivity and polarization loss of an insulation system [33, 37]. Hence, the real and imaginary parts of the complex capacitance of the oil-paper insulation grow, as displayed in Figure 8.

Table 6 exhibits the HDM parameter identification results of four insulation samples with different moisture content based on FDS test data obtained at 30 °C.

It can be seen from the table 6, Geometric capacitance C_g is immune to moisture content in the oil-paper insulation, owing to the structure and size of the oil-paper insulation system not being impacted by moisture content. This finding was acquired by analyzing the fitting model parameters under different moisture content. On the other hand, insulation resistance, R_g, is sensitive to the variation of moisture content. R_g trails off monotonously with the elevation of moisture content on account of the increased moisture content promoting the injection and migration of charged particles inside the medium more rapidly, which significantly improves the conductivity of oil-paper insulation. Meanwhile, polarization resistance, R_p, decreases, and polarization capacitance, C_p, increases monotonously with moisture content in the branch with the maximum time constant (the fifth branch in Table 6) by the principle that water molecules are highly polar molecules and tend to combine with hydrophilic groups to form charged ions. At the same time, water molecules promote the cracking of large insulating molecules in oil paper, resulting in an augment in the number of polarized molecules in the system, a strengthening in the capacity of dielectric bounding charge,

TABLE 6 Model parameter identification results of four different moisture content samples

				Polarizationbranch				
	Geometric equivalent circuit			RC series polarization branch		Interface polarization branch		
Moisture content (%)	R_g /GΩ	C_g/nF	Branch number	R_{pi}/GΩ	C_{pi}/nF	$R_{h(2j-1)}$/GΩ	$R_{h(2j)}$/GΩ	C_{hj}/nF
0.244%	1653.3428	0.014705	1	124.27461	0.07514785	46.6028	8461.7784	466.6426
			2	1592.0699	132.4243			
			3	1395.3932	615.6794			
			4	1578.937	249.9463			
			5	1431.4641	835.7335			
1.58%	798.0011	0.013274	1	66.56986	0.09119127	269.3966	136.7982	1.0777
			2	575.5306	0.02971042			
			3	611.5954	203.4712			
			4	659.4842	211.8623			
			5	745.8811	1530.2407			
2.77%	619.7557	0.016668	1	52.92751	0.11513645	778.9958	322.4799	604.2499
			2	219.4554	0.11927754			
			3	166.9357	10.498109			
			4	697.6509	1018.258			
			5	303.8621	2694.5345			
3.63%	511.5329	0.01961	1	47.82794	0.09258033	3055.6077	218.27547	197.4933
			2	166.2156	0.1169231			
			3	94.31908	20.8697			
			4	515.3104	772.7944			
			5	295.4524	2750.361			

TABLE 7 Consistency of the reconstructed fds curve based on four sets of model parameter identification results

Moisture content (%)	Consistency W_1 of C' (%)	Consistency W_2 of C'' (%)	Consistency W_3 of tan δ (%)
0.244%	95.64%	98.02%	94.06%
1.58%	97.39%	99.23%	95.93%
2.77%	98.26%	99.21%	96.97%
3.63%	98.52%	99.14%	98.01%

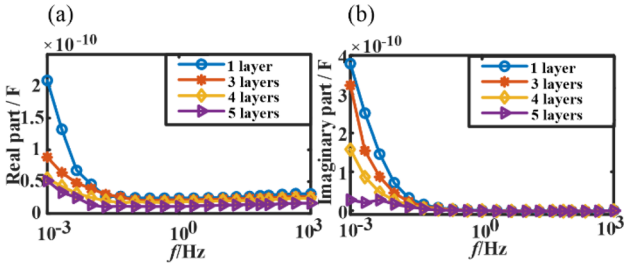

FIGURE 9 Complex capacitance curve under different insulation paper layers: (a) Real part; (b) imaginary part

and a deepening in the degree of polarization. Furthermore, charged ions formed through the combining of water molecules and hydrophilic groups facilitate large molecule cracking, multiply polarized molecules, and intensify the ability of dielectric bound charge, which are seen through the enhancement of the polarization extent, relative permittivity, as well as the descent of the corresponding polarization resistance and the ascent of the polarization capacitance. The influence laws of the growing moisture content on the complex capacitance are consistent with the effects of R_g, R_p, and R_b reductions (C_p and C_b increments) on the FDS characteristics simulated in Section 3, which verifies the validity of utilizing the HDM to simulate FDS characteristics of an oil-paper system.

Table 7 shows the consistency values of the FDS curve reconstructed by the identified parameters based on HDM oil-paper insulation samples with different moisture content and the original measurement curve.

In the Table 7, all the consistency values were above 94%, reflecting the feasibility and accuracy of the equivalent model constructed in this paper. It also proves that HDM can effectively reflect the polarization process of oil paper insulation system with different moisture content.

5.2 | Analysis of FDS data and HDM model parameters of oil paper insulation samples with different layers of insulating paper

Researching the FDS characteristics of different layers of insulation paper is a profitable means by which to obtain the FDS peculiarity of a transformer insulation system composed of a multilayer oil channel and insulation paper, as presented in Figure 9. The number of insulation paper layers in the test sample was set as 1, 3, 4, and 5 layers, and the testing ambient temperature was 30 °C. The test revealed that the real part of the complex capacitor moves downward with the augmentation of paper layers throughout the whole frequency band, while the imaginary part shifts down only in the low frequency band. Table 8 shows the HDM parameter identification results of four insulation samples with different insulation layers based on FDS test data obtained at 30 °C Insulation resistance R_g enlarges with the increase of the number of insulation layers, while geometric capacitance C_g decreases slightly.

During the period of dielectric charging between parallel plates, the complex capacitor can be described as:

$$C^* = \varepsilon_0 \varepsilon_r S/d \tag{8}$$

where ε_0, ε_r, S, and d are the vacuum dielectric constant, relative dielectric constant, plate area, and dielectric thickness, respectively. The real part of the complex capacitor declines on account of the growth of dielectric thickness d, in accompaniment with the multiplication of the insulation paper layers, according to Equation (8). However, the imaginary part of the complex capacitor remains constant, owing to the loss between the insulation cardboard and the number of insulation paper layers.

Table 9 demonstrates the consistency values of the FDS curve reconstructed using the identified parameters based on HDM oil-paper insulation samples with different numbers of insulation paper layers and the original measurement curve.

In the Table 9, all the consistency values were above 91%. The variation rules of the growing number of insulation paper layers on the complex capacitance are in accordance with the effects of C_g's reduction of the FDS characteristics simulated in Section III, which confirms that the characteristics of the complex capacitance's real part can reflect the deformation or burnout of the transformer winding. Diverse insulation system temperatures inside a transformer can be caused by the varying load of the transformer during operation or different seasons [37, 38]. It is also proved that HDM can effectively reflect the polarization process of oil paper insulation system with different shapes and structures.

5.3 | Analysis of FDS data and HDM model parameters of oil paper insulation samples at different temperatures

Figure 10 exhibits the conspicuous impact of different test temperatures on the FDS characteristics of the oil-paper insulation samples within 1% moisture content, measured at 40, 60, and 80 °C. The insulation paper of the test samples had five layers, and the moisture content was controlled within 1%. The real part and the imaginary part of the complex capacitor shift up with the ascent of the test temperature within the frequency

TABLE 8 Model parameter identification results of four different insulation paper layer samples

	Geometric equivalent circuit		Polarizationbranch				
			RC series polarization branch		Interface polarization branch		
Number of insulationpaper layers	R_g /GΩ	C_g/nF	Branch number	R_{pi}/GΩ	C_{pi}/nF	$R_{h(2j-1)}$/GΩ	$R_{h(2j)}$/GΩ	C_{hj}/nF
1 layer	1826.754	0.0525	1	345.814	0.0145	575.140	1011.313	0.4408
			2	572.391	0.0528			
			3	1845.607	677.652			
3 layers	1958.3543	0.034949	1	674.005	0.0382	2044.255	1703.204	1.4044
			2	1931.899	0.3516			
			3	1950.676	0.1675			
4 layers	3462.4883	0.016107	1	10282.68	0.0001	1094.812	3178.753	0.0304
			2	2765.935	0.1111			
			3	3416.712	245.120			
5 layers	3888.9623	0.010179	1	1677.440	0.0066	3648.588	10.0001	0.0304
			2	3114.999	0.0292			
			3	4127.740	1187.015			

TABLE 9 Consistency of the reconstructed fds curve based on four sets of model parameter identification results

Number of insulation paper layers	Consistency W_1 of C' (%)	Consistency W_2 of C'' (%)	Consistency W_3 of tan δ (%)
1 layer	95.93%	91.04%	91.76%
3 layers	93.39%	95.54%	91.95%
4 layers	96.26%	95.94%	96.77%
5 layers	93.02%	92.87%	94.15%

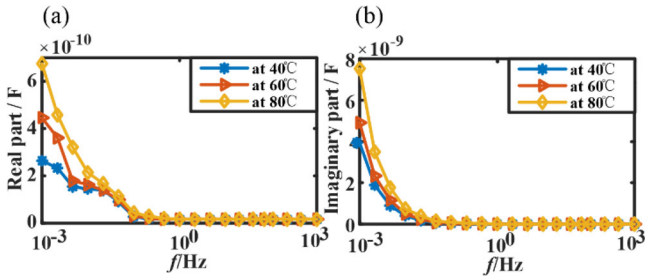

FIGURE 10 Complex capacitance curve at different test temperatures: (a) Real part; (b) imaginary part

range of 10^{-3}–10^{0} Hz, and simultaneously, neither is significantly altered by the test temperature in the high frequency range.

The HDM parameter identification results of three insulation samples based on FDS test data tested at diverse temperatures are displayed in Table 10.

It can be seen from the Table 10, geometric capacitance C_g depends on the structure and size of the oil-paper insulation system, remains invariant or float very slightly at various test temperatures, and cannot transform the insulation structure. Dissimilarly, insulation resistance R_g is susceptible to the variation of the surrounding temperature, leading to its diminution in the case of an upward trend in temperature. Furthermore, polarization resistance R_p decreases, and polarization capacitance C_p increases, monotonously with the moisture content in the branch with the maximum time constant (the fifth branch in Table 10).The variation rules lie in the mechanism where the escalation of the temperature aggravates the thermal motion of polar molecules, accelerates the relaxation process, shortens the relaxation time, enhances the polarization intensity of the system, elevates the polarisability, promotes the Carrier migration rate of the system, magnifies the conductivity, and strengthens the conductance process.

Table 11 displays the consistency values of the FDS curve reconstructed using the identified parameters based on HDM oil-paper insulation samples with different test temperatures and the original measurement curve.

It can be seen from the Table 11, all the consistency values were above 92%. And the influence laws of the growing test temperature on the complex capacitance are consistent with the effects of R_g, R_p, and R_b reductions (C_p and C_b increments) on the FDS characteristics simulated in Section 3, which verifies that HDM can effectively reflect the polarization process of oil paper insulation system under different test temperatures.

6 | CONCLUSION

This paper used the hybrid Debye model to analyses the hybrid polarization frequency domain spectrum characteristics of oil-paper insulation systems under different conditions through

TABLE 10 Model parameter identification results of three oil-paper insulation samples at different test temperature

	Geometric equivalent circuit			Polarizationbranch				
				RC series polarization branch		Interface polarization branch		
Test temperature (°C)	R_g /GΩ	C_g/nF	Branch number	R_{pi}/GΩ	C_{pi}/nF	$R_{h(2j-1)}$/GΩ	$R_{h(2j)}$/GΩ	C_{hj}/nF
40°C	676.6278	0.03253	1	19.18494	0.105514	196.2462	0.0001	47.71
			2	632.0543	0.127289			
			3	505.7744	279.102			
			4	88.24244	2992.33			
			5	443.1531	515.888			
60°C	475.1938	0.066788	1	197.0047	0.2516256	452.64027	3095.4546	24.6592
			2	249.8215	34.50617			
			3	451.2693	19.15827			
			4	374.996	73.68039			
			5	221.3471	534.4172			
80°C	411.8379	0.027109	1	13.03983	0.1572824	28.515203	4742.4804	176.3433
			2	147.4687	0.269948			
			3	407.9868	11.60249			
			4	374.996	12.6651			
			5	221.3471	605.7437			

TABLE 11 Consistency of the reconstructed fds curve based on three sets of model parameter identification results

Test temperature	Consistency W_1 of C' (%)	Consistency W_2 of C'' (%)	Consistency W_3 of tan δ (%)
40 °C	92.46%	95.49%	94.80%
60 °C	97.66%	96.73%	93.87%
80 °C	94.28%	97.27%	93.35%

simulation and experiments. The findings can be summarised as follows:

1. FDS simulation results disclose that the variation of the parameters in each branch of the hybrid Debye model of oil-paper insulation can simulate the oil-paper insulation aging process, which was presented regularly on the frequency domain curves of the complex capacitance.
2. The experimental results show that the complex capacitance and dielectric loss factor of the oil-paper insulation system change with the moisture content, the layers of insulating paper, and the test temperature, and are reflected in the corresponding HDM parameters. In addition, using the HDM parameters of the oil-paper insulation samples under different conditions to reconstruct the FDS curve and the original measurement curve has a higher consistency value, which further proves that HDM can effectively reflect the hybrid polarization of the oil-paper insulation system.
3. The parameters of HDM are sensitive to the variation of external factors, and can be used as characteristics for non-destructive evaluation of oil-paper insulation state.

ACKNOWLEDGMENTS

The authors thank the Natural Science Foundation of Fujian under Grant 2019J01248 and the Science Development Foundation of Fuzhou University under Grant GXRC-18070 for the financial support provided. The authors also thank the anonymous editor and the reviewers' accurate and valuable comments on the manuscript.

REFERENCES

1. Jadav, R.B., Ekanayake, C., Saha, T.K.: Understanding the impact of moisture and ageing of transformer insulation on frequency domain spectroscopy. IEEE Trans. Dielectr. Electr. Insul. 21(1), 369–379 (2014)
2. Mikulecky, A., Stih, Z.: Influence of temperature, moisture content and ageing on oil impregnated paper bushings insulation. IEEE Trans. Dielectr. Electr. Insul. 20(4), 1421–1427 (2013)
3. Liao, R., et al.: Quantitative analysis of insulation condition of oil-paper insulation based on frequency domain spectroscopy. IEEE Trans. Dielectr. Electr. Insul. 22(1), 322–334 (2015)
4. Mishra, D., et al.: Use of Interfacial Charge for Diagnosis and Activation Energy Prediction of Oil-Paper Insulation Used in Power Transformer. IEEE Trans. Power Delivery 34(4), 1332–1340 (2019)
5. Yang, X., Nielsen, S., Ledwich, G.: Investigations of dielectric monitoring on an energised transformer oil–paper insulation system. IET Sci. Meas. Technol. 9(1), 102–112 (2015)
6. Lin, Y., et al.: Aging assessment of oil-paper insulation of power equipment with furfural analysis based on furfural generation and partitioning. IEEE Trans. Power Delivery 34(4), 1626–1633 (2019)

7. Sarkar, S., et al.: An expert system approach for transformer insulation diagnosis combining conventional diagnostic tests and PDC, RVM data. IEEE Trans. Dielectr. Electr. Insul. 21(2), 882–891 (2014)
8. Wolny, S.: Aging degree evaluation for paper-oil insulation using the recovery voltage method. IEEE Trans. Dielectr. Electr. Insul. 22(5), 2455–2462 (2015)
9. Saha, T.K., Purkait, P., Müller, F.: Deriving an equivalent circuit of transformers insulation for understanding the dielectric response measurements. IEEE Trans. Power Delivery 20(1), 149–157 (2005)
10. Wolny, S., Zdanowski, M.: Analysis of recovery voltage parameters of paper-oil insulation obtained from simulation investigations using the Cole-Cole model. IEEE Trans. Dielectr. Electr. Insul. 16(6), 1676–1680 (2009)
11. Suriyah-Jaya, M., Leibfried, T.: Accelerating dielectric response measurements on power transformers—part II: A regression approach. IEEE Trans. Power Delivery 29(5), 2095–2110 (2014)
12. Saha, T.K., Purkait, P.: Investigation of polarization and depolarization current measurements for the assessment of oil-paper insulation of aged transformers. IEEE Trans. Dielectr. Electr. Insul. 11(1), 144–154 (2004)
13. Roongroj, C., et al.: Equivalent circuit approximation of transformer insulation by using PDC measurement. In: *Proceedings of the IEEE International Conference on Electrical Engineering/Electronics*, Krabi, Thailand, pp. 925–928 (2008)
14. Banerjee, C.M., et al.: Influence of charging voltage magnitude on time domain dielectric response of oil–paper insulation. IET Sci. Meas. Technol. 13(6), 874-882 (2019)
15. Liao, R., et al.: Quantitative diagnosis of moisture content in oil-paper condenser bushing insulation based on frequency domain spectroscopy and polarisation and depolarisation current. IET Gener. Transm. Distrib. 11(6), 1420–1426 (2017)
16. Fofana, I., et al.: Polarization and depolarization current measurements of oil impregnated paper insulation system under thermal runaway. In: *Proceedings of the IEEE International Conference on Solid Dielectrics*, Germany, pp. 1–4 (2010)
17. Pradhan, A.K., Chatterjee, B., Chakravorti, S.: Effect of temperature on frequency dependent dielectric parameters of oil-paper insulation under non-sinusoidal excitation. IEEE Trans. Dielectr. Electr. Insul. 21(2), 653–661 (2014)
18. Gao, J., et al.: Condition Diagnosis of Transformer Oil-paper Insulation Using Dielectric Response Fingerprint Characteristics. IEEE Trans. Dielectr. Electr. Insul. 23(2), 1207–1218 (2016)
19. Wang, W., et al.: Effect factors analysis of frequency domain spectroscopy test. In: *Proceedingsof the IEEE Asia-Pacific Power and Energy Engineering Conference*, Shanghai, China, pp. 1–5 (2012)
20. Jaya, M., Geißler, D., Leibfried, T.: Accelerating dielectric response measurements on power transformers—part I: A frequency-domain approach. IEEE Trans. Power Delivery 38(3), 1469–1473 (2013)
21. Pradhan, A.K., et al.: Determination of optimized slope of triangular excitation for condition assessment of oil-paper insulation by frequency domain spectroscopy. IEEE Trans. Dielectr. Electr. Insul. 23(3), 1303–1012 (2016)
22. Pradhan, A.K., Chatterjee, B., Chakravorti, S.: Estimation of paper moisture content based on dielectric dissipation factor of oil-paper insulation under non-sinusoidal excitations. IEEE Trans. Dielectr. Electr. Insul. 22(2), 822–830 (2015)
23. Betie, A., et al.: Neural network approach to separate aging and moisture from the dielectric response of oil impregnated paper insulation. IEEE Trans. Dielectr. Electr. Insul. 22(4), 2176–2184 (2015)
24. Mishra, D., et al.:Effect of charge accumulated at oil–paper interface on parameters considered for power transformer insulation diagnosis. IET Sci. Meas. Technol. 12(3), 411–417 (2018)
25. Bognar, A., et al.: Spectrum of polarization phenomena of long time-constant as a diagnostic method of oil-paper insulating system. In: *Proceedingsof the IEEE International Conference on Properties and Applications of Dielectric Materials,* Tokyo, Japan, pp. 723–726 (1991)
26. Liang, G., et al.: Modelling of frequency characteristics of the oil-paper compound insulation based on the fractional calculus. IET Sci. Meas. Technol. 11(5), 646–654 (2017)
27. Mishra, D., et al.: Assessment of interfacial charge accumulation in oil-paper interface in transformer insulation from polarization-depolarization current measurements. IEEE Trans. Dielectr. Electr. Insul. 24(3), 1665–1673 (2017).
28. Patsch, R., Kouzmine, O.: P-factor, a meaningful parameter for the evaluation of return voltage measurements. In: *Proceedingsof the IEEE Annual Report Conference on Electrical Insulation and Dielectric Phenomena*, Cancun, Mexico, pp. 906–909 (2002)
29. Patsch, R., Menzel, J.: Ageing and degradation of power transformers — how to interpret return voltage measurements. In: *Proceedingsof the IEEE International Symposium on Electrical Insulating Materials,* Yokkaichi, Japan, pp. 179–182 (2008)
30. Zhang, M., et al.: Modelling the low-frequency electrode dielectric response based on transformer equivalent oil-paper insulation model. IET Sci. Meas. Technol 13, 700–707 (2019)
31. Ojha, S.K., et al.: Application of Cole–Cole model to transformer oil-paper insulation considering distributed dielectric relaxation. High Voltage 4, 72–79 (2019)
32. Dey, D., et al.: Effect of measurement temperature on interfacial charge freed from deep traps located at the interface of oil-paper insulation. In: *Proceedingsof the IEEE Applied Signal Processing Conference,* Kolkata, India, pp. 346–350 (2018)
33. Zhang, D., et al.: Study on FDS characteristics of oil-immersed paper insulation bushing under non-uniform moisture content. IET Sci. Meas. Technol. 12(5), 691–697, (2018)
34. Rajput, V., et al.: Effect of introduced charge on frequency domain dielectric response of oil-paper insulation. In: *Proceedingsof the IEEE Calcutta Conference,* Kolkata, India, pp. 125–129 (2017)
35. Yang, L., et al.: Dielectric response measurement of oil-paper insulation based on system identification and its time-frequency-domain conversion method. IEEE Trans. Dielectr. Electr. Insul. 25(5), 1688–1698 (2018)
36. Meghnefi, F., et al.: Deriving an equivalent circuit of composite oil paper insulation for understanding the frequency domain Spectroscopic measurements. In: *Proceedingsof the IEEE Conference on Electrical Insulation and Dielectric Phenomena*, Virginia Beach, pp. 478–481 (2009)
37. Ansari, M.A., Martin, D., Saha, T.K.: Investigation of distributed moisture and temperature measurements in transformers using fiber optics sensors. IEEE Trans. Power Delivery 34(4), 1776–1784 (2019)
38. Wang, L., et al.: Aging characteristic parameter extraction of oil-paper insulation based on frequency domain spectroscopy. In: *Proceedings of the IEEE International Conference on Condition Monitoring and Diagnosis* , Xi'an, China, pp. 968–971 (2016)

How to cite this article: Zou Y, He J, He Q, Wang M. Analysis of hybrid polarization frequency domain spectrum characteristics of oil-paper insulation transformers. IET Sci. Meas. Technol. 2021;15:653–662. https://doi.org/10.1049/smt2.12066